Commissioning, performance benchmarking, and investigation of alkali emissions in a 10 kWth solid fuel chemical looping combustion pilot

Fuel 287 (2021) 119530

Contents lists available at ScienceDirect

Fuel

journal homepage: www.elsevier.com/locate/fuel

Full Length Article

Commissioning, performance benchmarking, and investigation of alkali emissions in a 10 kW_{th} solid fuel chemical looping combustion pilot

Ivan Gogolev *, Amir H. Soleimanisalim, Carl Linderholm, Anders Lyngfelt

Department of Space, Earth and Environment, Chalmers University of Technology, Hörsalsvägen 7b, 412 96 Gothenburg, Sweden

ARTICLE INFO

Keywords:
Chemical looping combustion
Biomass
Alkali
Surface ionization detector
Bio-energy with carbon capture and storage

ABSTRACT

Chemical looping combustion of biomass-sourced fuels (bio-CLC) is a novel bio-energy with carbon capture and storage (BECCS) technology for power and heat generation with net negative CO_2 emissions. In this study, a new 10 kW_{th} CLC pilot designed for high-volatiles biomass fuels was commissioned with ilmenite oxygen carrier and five different biomass fuels of varying volatile and alkali content fractions. The system was tested for its ability to convert high and low volatile content biomass, while achieving high carbon capture efficiency. The new pilot achieved carbon capture close to 100% for high-volatiles biomass, and >94% for low-volatiles biomass char fuels. Furthermore, due to the implementation of a volatiles distributor, the new pilot demonstrated an improvement of up to 10 percentage points of gas conversion efficiency for high-volatiles biomass vs. the previous generation reactor. Gaseous alkali emissions were measured with a surface ionization detection system. Flue gas alkali release levels were found to rise with higher fuel alkali content. Alkali emissions were found to be approximately similar in the AR and the FR for all but the straw pellet mixture fuel (highest alkali content fuel). For the straw pellet mixture, gaseous alkali release levels in the AR were up to seven times higher than those of the FR. In all cases, over 96% of the fuel's alkalis were absorbed by the ilmenite bed material. Ilmenite's strong alkali absorption characteristics were concluded to be the key determinant of gas-phase release of biomass alkali in the conducted experiments.

1. Introduction

Chemical looping combustion (CLC) is promising thermal fuel conversion technology that allows low-cost and low-energy-penalty integrated carbon capture [1]. The principle of CLC is shown in Fig. 1 and consists of cyclical oxidation and reduction of a metal oxide material, the oxygen carrier (OC), circulated through two-interconnected reactors. The metal oxide is reduced by fuel in the fuel reactor (FR) and oxidized by air in an air rector (AR). In this process scheme, oxygen is transferred by the OC from the air in the AR to the fuel in FR, while nitrogen is rejected in the AR. Thus, fuel in the FR is converted with pure oxygen, resulting in a nitrogen-free flue gas. This avoids the costly separation of CO_2 from nitrogen that is required in post-combustion CO_2 capture systems. A more complete overview of the CLC process is described in several review publications [2–6].

Until the early 2000's CLC was largely a paper concept, until the first successful pilot-scale demonstration of the process in 2004 [7]. Since then the field of chemical looping has grown, with multiple research teams addressing process optimization, oxygen carrier material screening and development, thermodynamic and kinetics studies of the process, as well as the adoption of the CLC principle for development of novel related technologies such as chemical looping reforming, chemical looping gasification, oxygen carrier aided combustion, and others [4,8,9]. The technology readiness level (TRL) of chemical looping combustion technology is currently at TRL6 [10]. Pilot work remains the ultimate test for the study, development, and validation of the CLC process. Since the first demonstration of CLC technology, at least 46 CLC pilot rectors have been successfully constructed and operated with gaseous, liquid, and solid fuels [11].

In recent years, the use of biomass as fuel in CLC (bio-CLC) has been of great interest. Bio-CLC is a bioenergy with carbon capture and storage (BECCS) technology that allows for a net negative CO_2 emissions impact. Since negative emissions technologies (NETs) are deemed necessary for achieving ambitious CO_2 emissions reduction targets, as indicated in the Fifth Assessment Report of the Intergovernmental Panel on Climate Change (IPCC) [12], development of bio-CLC is highly relevant. Although CLC with solid fuels has been demonstrated in various pilots using fossil-derived fuels, CLC of biomass remains a relatively unexplored area of the CLC suite of technologies. In a recent review by Lyngfelt et al. [11], of the 22 pilot CLC systems capable of using solid fuels, less than half of the pilot systems have been operated using

* Corresponding author.

https://doi.org/10.1016/j.fuel.2020.119530
Received 22 July 2020; Received in revised form 11 September 2020; Accepted 15 October 2020
Available online 5 November 2020

Nomenclature

AR	air reactor
BECCS	bioenergy with carbon capture and storage
bio-CLC	biomass chemical looping combustion
BP	black pellets
BT	benchmarking test
CLC	chemical looping combustion
CLOU	chemical looping with oxygen uncoupling
CPC	condensation particle counter
FR	fuel reactor
GWC	German wood char
IPCC	intergovernmental panel on climate change
LLS	lower loop seal
NDIR	non-dispersive infrared
NETs	negative emissions technologies
OC	oxygen carrier
PFR	pine forest residue
SMPS	scanning mobility particle sizer
SPM	straw pellet mixture
SID	surface ionization detector
SWC	Swedish wood char
TC	thermal conductivity
TRL	technology readiness level
ULS	upper loop seal
$m_{oc,i}$	mass of oxygen carrier in section i, in kg
A_i	cross-sectional are of section i, in m^2
ΔP_i	pressure drop over section i, in Pa
g	gravitational constant in, N/kg
CI	dimensionless circulation index
$\dot{Q}_{i,j}$	flow of gas i in section j, in m^3_{normal}/min
η_{oo}	oxide oxygen efficiency, in %
$x_{i,j}$	mole fraction of gas i in reactorj
d	dimensionless nitrogen dilution ratio
Ω_{OD}	oxygen demand, in %
$\eta_{gas\ conv.}$	gas conversion efficiency, in %
DR_j	dimensionless dilution ratio in reactor j
Φ_o	ratio of moles of O_2/kg of fuel to moles of C/kg of fuel
$K_{accum.\ by\ OC}$	potassium accumulated by the OC, in g
$K_{input\ by\ fuel}$	potassium input with fuel, in g

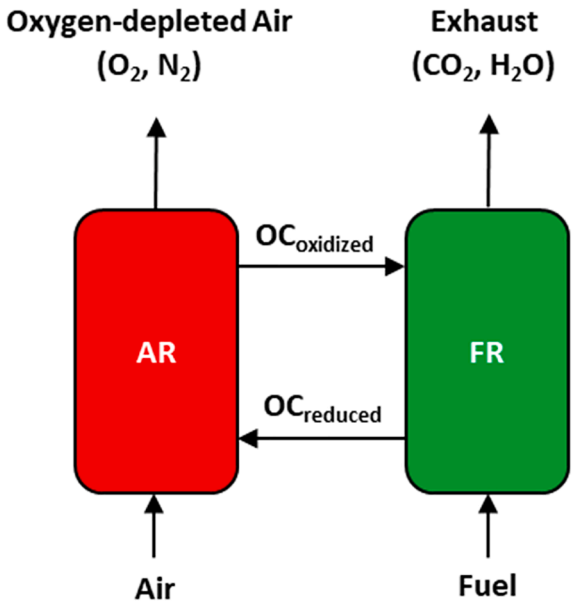

Fig. 1. Chemical looping combustion process simplified schematic.

biomass. For most of these units, the original design was developed for general solid fuel capability, with coal as the basis fuel. Although such units are capable of operation with biomass, their design is not optimal for the relatively high volatile content of biomass fuels.

The aim of this study was to commission and establish performance benchmarks of a new 10 kW_{th} CLC pilot designed specifically for conversion of high-volatiles fuels such as biomass. Furthermore, this study aimed to develop the understanding of how alkalis that are found in higher proportion in biomass fuels will influence the CLC process. In conventional fluidized bed combustion of biomass, alkalis are well-known to cause corrosion and fouling of heat exchange equipment and agglomeration of the bed material. The behavior of alkali release and how alkalis influence the CLC process remains largely unexplored. The determination of this behavior is integral to development of bio-CLC systems and is addressed in this study.

2. Background

Design of CLC pilot systems for solid fuel conversion must address several unique challenges not encountered in CLC of gaseous fuels. The main difference is that solid fuels undergo rapid devolatilization, leaving behind solid char. While devolatilized species can react upon contact with the OC, the char must first be gasified by steam or CO_2 in order to form gasification products that can react upon contact with the OC. Fuel composition plays a large role here. Solid fossil fuels, such as coal and coke, typically have a relatively low volatiles content, but high char content, as compared to biomass. For such fuels, char gasification is the rate-limiting step in the overall fuel conversion process [6,13]. To achieve high char conversion and to prevent loss of char to the AR, the pilot system must maximize char contact with steam and the OC. The OC circulation rate and the FR inventory control the OC residence time in the FR. The OC residence time, in-turn, affects char residence time, and thus directly influences char conversion. However, OC circulation is constrained by the energy balance and FR inventory is subject to practical limitations. Given these constraints, another option to influence char conversion is to reduce the fuel size. For a given OC residence time, smaller fuel particles improve char conversion. For example, an optimum size for coal fuel is in the size range of 100–300 μm [6]. Reduction of the fuel size also has limitations as particles that are too small can be stripped by the fluidizing gas and carried away unconverted with the FR flue gas. To limit char elutriation, some pilot unit designs have opted to add a char separation loop, called a carbon stripper, to the FR. The purpose of a carbon stripper is to separate char from the OC leaving the FR and recirculate it back to the FR for further conversion.

Biomass fuels behave differently from solid fossil-derived solid fuels. Depending on the type, biomass fuels typically have a volatile content of 60–85 wt% [14]. The high proportion of volatiles and the quick nature of devolatilization results in suboptimal contact of the volatiles with the OC. This results in incomplete conversion. Complete conversion requires post-injection of oxygen to the FR flue gas in order to complete the oxidation. To improve the contact between volatiles and the OC, fuel feeding into the bottom of the FR bed is preferred. Oxygen carriers capable of releasing free oxygen in the FR have also been used. Use of such oxygen carriers is classified as a subset of chemical looping technology, termed chemical looping with oxygen uncoupling (CLOU). The oxygen release from CLOU oxygen carrier enhances conversion, as some free oxygen is available for oxidation of unconverted volatiles in the

freeboard of the FR. Nevertheless, typical gas conversion efficiency reported for bio-CLC reactor operation are below 80%, and improvement of gas conversion efficiency is pursued with testing of alternative oxygen carriers or with new CLC pilot designs.

Further to influencing conversion, the high volatiles fraction of biomass fuels means that the char content of biomass is significantly lower than that of fossil-derived solid fuels. Biomass char is more reactive than that of fossil fuel char, and thus easier to gasify. The increased reactivity of biochar is attributed to the alkali content of biomass and biochar's increased porosity and surface area, when compared to char originating from fossil-derived solid fuels. Alkali, K and Na, are known catalysts for char gasification [15]. The increased porosity and active surface area also improve gasification, since char gasification depends on surface reactions [16–18]. The lower relative amount and higher reactivity of biomass char alleviates the design challenge encountered with fossil-derived fuels in CLC, leaving the issue of volatiles conversion as the primary reactor design issue.

The first CLC reactor for solid fuels was designed and commissioned by Berguerand and Lyngfelt in 2008 at Chalmers University of Technology and is described in detail in [19]. From 2011, results from other solid-fuel-capable reactors began to appear in published literature. Most of these designs use a high-velocity riser AR and either a bubbling bed or a high velocity riser as the FR. Most of these CLC pilots were designed for general solid fuel conversion with coal as the basis fuel. Operational experience from the original Chalmers 10 kW solid fuels reactor as well as published results from other solid fuel CLC pilot units confirms that the primary challenge in bio-CLC is poor volatiles conversion.

Another key consideration for designing a pilot system for biomass CLC is the release of alkali during fuel conversion. Compared to fossil-based solid fuels, biomass typically has less ash, but can contain higher levels of alkalis (Na and K), as they are essential nutrients for plant growth [14]. In conventional combustion of biomass in boilers, alkalis are known to cause severe issues in for heat exchange surfaces, as well as in the boiler bed. Alkalis are released to the gas phase at temperatures above 700 °C. The release is primarily facilitated by Cl through formation of highly volatile KCl and NaCl salts that cause fouling and corrosion of the heat exchange equipment [16,20]. Alkali species can also be retained in the ash fraction of the bed, where they can react to form potassium and sodium silicates. At process conditions, these species form sticky melts that initiate agglomeration of bed material.

In CLC, the fate of alkali release is largely unknown. Several studies have reported observations of interaction of biomass alkali with oxygen carriers. In a 1 kW pilot CLC study with wood saw dust fuel and iron oxygen carrier, Gu et al. found that alkalis form deposits on the OC but do not affect its reactivity [21]. In similar experiments in a 500 W CLC pilot, Mendiara et al. found no deposition or effect on reactivity of the iron ore OC [22]. In experiments with ilmenite, the most common OC for solid fuels, Corcoran et al. has shown that ilmenite absorbs alkali, thus limiting the release to the gas phase, as well as preventing formation of alkali silicates [23]. To date, literature mentions only one study that has reported alkali gas phase release measurements in CLC [24].

3. Experimental setup

3.1. New reactor design

Following on operational experience gained from operating the original Chalmers 10 kW solid fuels reactor with 5 different fossil-derived fuels, 4 biomass fuels, and 8 different oxygen carriers [19,25–32] a new design of a 10 kW solid fuels reactor was proposed in 2014. It was designed and constructed in 2018–2019 and commissioned in November of 2019. The reactor consists of an interconnected high velocity riser AR and a bubbling fluidized bed FR. The AR outlet is equipped with a cyclone to separate OC particles from the AR flue gas. The upper loop seal (ULS) between the cyclone dip leg and the FR, and the lower loop seal (LLS) between the FR overflow and the AR, are used to prevent gas leakage between the reactors. The design of this unit was largely based on the arrangement and geometry of the original unit, but incorporates important modifications aimed at improving performance, reliability, as well as to directly address issues with high volatiles content of biomass. These modifications include:

- No carbon stripper on the FR – a carbon stripper was deemed not critical for biomass as the fuel char fraction is lower and the char is more reactive (vs. fossil-derived solid fuels).
- FR volume is larger – this will give a longer residence time to promote good char conversion and avoid char carryover to the FR.
- Volatiles distributor – a perforated distributor has been added to the internals of the FR to promote contact of volatiles with the OC (discussed further in Section 3.2).
- Higher overflow in loop seals – the overflow height of the loop seals was made higher, enabling the loop seals to withstand a higher differential pressure between the AR and FR (prevents loop seal blowout and leakage).
- Solid sampling – the capability to sample the OC from the lower loop seal during operation was added.
- Alkali sampling – a flue gas sampling and measurement system based on the principle of surface ionization detection, with ability to sample from the FR and AR chimneys, was added to the reactor system (discussed further below).
- More robust design – the construction of the reactor was made more robust with reinforced flange connections and pressure tap connections.

Fig. 2 shows a schematic of the new 10 kW reactor design. Table 1 provides a summary of the new reactor's geometry, and Table 2 summarizes the normal operating parameters of the reactor.

The AR of the new system is geometrically identical to the previous design and consists of a high velocity riser with a wider base. The FR is a bubbling fluidized bed, as in the previous design. However, the FR volume was designed to be over 2 times larger than the previous design. This was done to increase OC and fuel residence time in order to aid char conversion. The bed height is approximately 1.5 times taller than the previous design, and should increase time for contact of the volatiles with the OC.

The solid fuel injection system from the first generation reactor was re-used in the present design. It consists of a closed hopper that is equipped with a rotary agitator which continuously mixes the fuel at the bottom of the hopper, and a double-screw feeder which conveys the solid fuel from the bottom of the hopper to a vertical fuel chute. The vertical fuel chute leads the fuel to the bottom section of the FR, where the fuel mixes with the bed material. To aid the feeding process, nitrogen sweep gas is supplied to the lid of the fuel hopper and to the top of the fuel chute.

3.2. Volatiles distributor

The most significant change implemented in this new reactor design is the addition of a volatiles distributor to the FR internals. Fig. 3 shows a section view of the FR along with a visualization of the volatiles distributor concept.

The idea behind the volatiles distributor is to optimize contact between biomass volatiles and the oxygen carrier. Experience with biomass fuels shows that devolatilization is a fast process. It is expected that as soon as biomass fuel is introduced into the fuel chute, it would heat up and start to devolatilize. Since the steam fluidizing velocity is several times higher than the OC minimum fluidization velocity, the additional volatile release would tend to pass though the bed as large bubbles, thus avoiding much of the close contact with the OC that is needed for conversion. The volatiles distributor is essentially a perforated internal baffle which separates much of the volatiles flow into

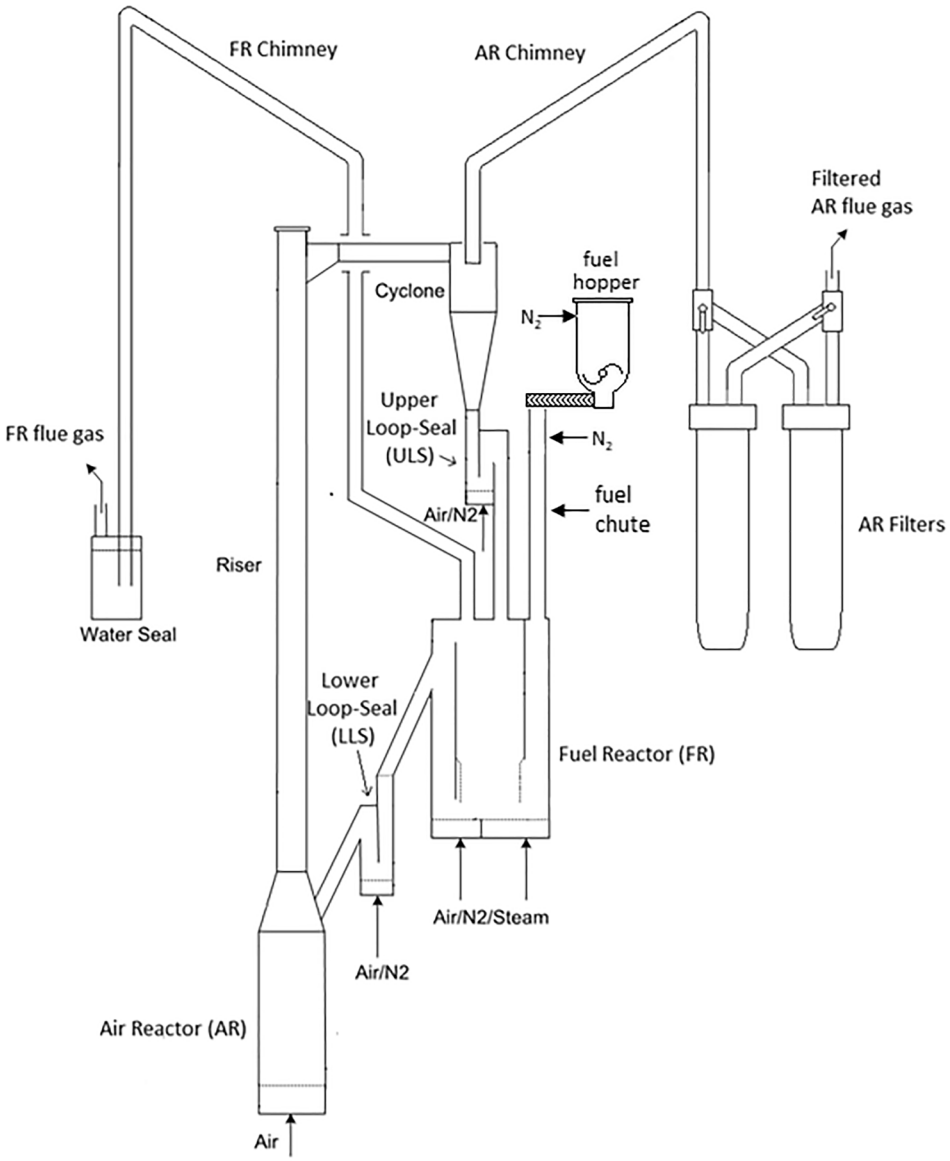

Fig. 2. Simplified schematic of the new 10 kW solid fuels CLC system.

Table 1
New 10 kW solid fuels CLC system key dimensions.

Reactor section	Dimensions (mm)	Area (cm^2)	Bed volume (cm^3)
AR – Bottom Section	154.08 mm ID × 356 mm high	186.3	n/a
AR – Conical Transition	88 mm high	variable	n/a
AR – Riser	62.71 mm ID × 1451 mm high to bottom of riser exit	30.9	n/a
Upper Loop Seal	104 mm × 54 mm × 180 mm high to overflow bottom	56.2	1 011
Fuel Reactor	234 mm × 85 mm × 408 mm high to overflow bottom	198.9	8 115
Lower Loop Seal	104 mm × 54 mm × 167 mm high to overflow bottom	56.2	938
Total Bed Volume Excluding the AR (cm^3)			10 064

multiple streams, thus increasing contact with the OC bed. It should be noted that the center section of the volatiles distributor remains open, such as not to impede fluidization and OC circulation in the FR.

Table 2
New 10 kW solid fuels CLC system key operating parameters.

Operating parameter	Normal operating value
AR Temperature (°C)	1000
AR Air Flow Rate (nL/min)	200
AR Riser Fluidization Velocity (m/s)	5.03
FR Temperature (°C)	975
Steam Flow Rate (g/min)	26.0
FR Mean Fluidization Velocity (m/s)	0.124
Loop Seal Nitrogen Flow Rate (nL/min)	10.0
Loop Seal Fluidization Velocity (m/s)	0.138

3.3. Flue gas alkali measurement system

The new 10 kW reactor was equipped with a flue gas alkali emissions measurement system. The schematic of this system is shown in Fig. 4.

The setup shown in Fig. 4 is capable of sampling the FR and AR flue gas. However, only one reactor can be sampled at a time. Raw flue gas from the FR and AR is sampled at approximately 900–1000 °C. At these process temperatures, the alkali species of concern are present in the gas phase, negating the need for isokinetic sampling. The raw flue gas is

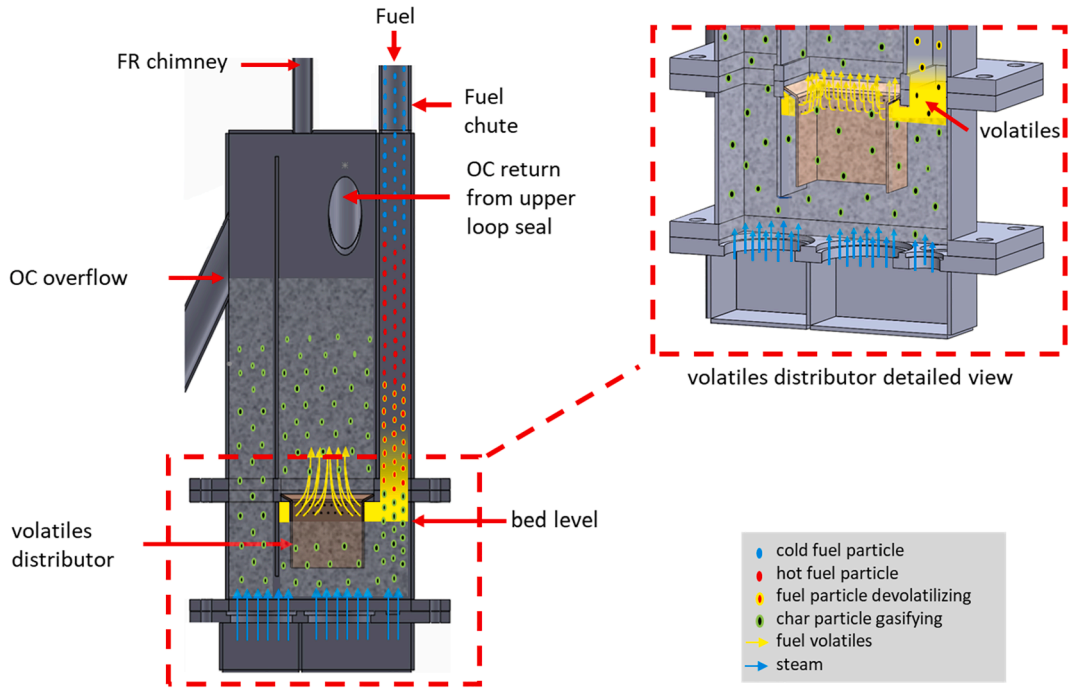

Fig. 3. Fuel reactor and volatiles distributor section view.

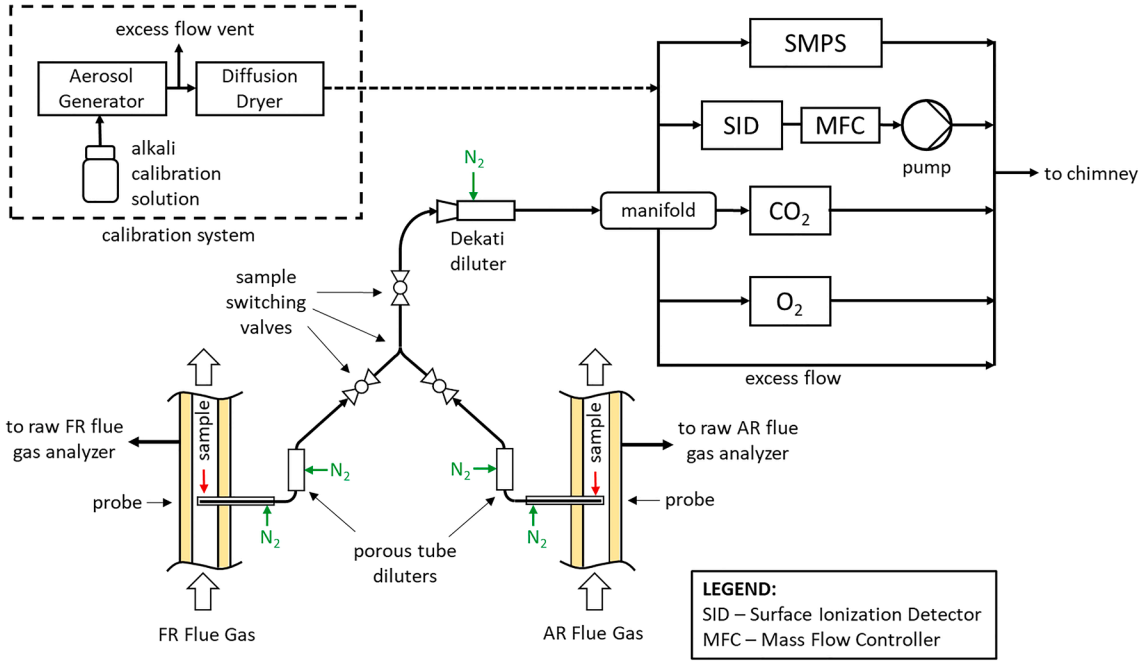

Fig. 4. Flue gas alkali measurement system schematic.

continuously sampled through a probe and diluted in three stages with nitrogen. The first stage of dilution occurs inside the sampling probe which is mounted perpendicularly to the flue gas flow. The probe's sample suction direction is set opposite of the flue gas flow in order to minimize ingress of OC fines – fine particles that originate from attrition and entrainment of the OC into the flue gases. The second stage of dilution is achieved in a porous flow diluter, and the third stage in a Dekati ® venturi-type diluter. The Dekati® diluter creates the suction necessary for sampling and provides positive pressure of the diluted sample at its outlet. Dilution is carried out to dilute and cool the sample flow such that alkali species in the gas phase nucleate into solid aerosol particles. This sample conditioning step is critical for minimizing condensation of alkali vapors onto the sampling tube walls and for improving the alkali measurement sensitivity of the surface ionization detector (SID).

From the Dekati® diluter, the diluted sample is split up through a manifold between a scanning mobility particle sizer (SMPS - TSI 3082 & CPC 3750), the surface ionization detector (SID), a CO_2 analyzer (LICOR LI-850), a trace oxygen analyzer (Alpha Omega Instruments 3000-Y230BTP), and a vent line for excess sample flow. The SID was custom built for this reactor and is the main measurement component that detects total flue gas alkali concentration using the principle of surface

ionization. The SID principle has been successfully used to measure alkali emissions in conventional combustion [33], gasification [34], and tested in a previous campaign on the Chalmers 100 kW CLC reactor [24]. A comprehensive overview of the SID's working principles is described in several publications [35,36]. The trace CO_2 analyzer is used to track overall dilution of the sample when measuring alkali in the FR flue gas. Since the FR raw flue gas CO_2 concentration is measured by the main process gas analyzers, the dilution ratio can be calculated by dividing the raw flue gas CO_2 concentration by the CO_2 concentration of the diluted sample. The dilution ratio is then used to recalculate the raw flue gas alkali concentration from the diluted sample alkali concentration measured by the SID. When measuring alkali levels in the AR flue gas, oxygen is used to track dilution. The undiluted AR flue gas oxygen concentration is measured by the main process gas analyzers, while oxygen in the diluted sample is measured by the trace oxygen analyzer. The SMPS system measures the concentration and distribution of particles in the diluted sample in the range of approx. 10–700 nm. It is primarily used for calibration of the SID. The SID is calibrated with a 0.005 M $KCl_{(aq)}$ solution. An aerosol generator uses the calibration solution to create fine aqueous KCl aerosol. This aerosol is dried in a diffusion dryer to precipitate solid KCl particles in the size range of approx. 10–600 nm. The calibration aerosol flow is then split between the SMPS system and the SID. The mass concentration of the KCl particles is calculated by the SMPS and compared to the SID output signal in order to create a calibration curve. SID instrument calibration for this campaign was performed at the beginning as well as after campaign completion. Deviation between the calibration results indicated that the SID instrument had an approximate measurement drift of up to + 1.5% per hour of operation. Although the SID's signal drift is not the only source of source of measurement uncertainty, the performance of the instrument was deemed acceptable for the comparison of time-averaged values utilized in the results and discussion sections.

3.4. Analytical methods

In addition to the alkali emissions measurement system described in Section 3.3, the key analytical methods employed in the study consist of reactor flue gas analysis. Gas composition for the AR and FR was determined by multicomponent gas analyzers. During operation, FR flue gas is continuously sampled from the FR chimney. The sample gas is first passed through a water-cooled condenser to reject majority of the water. The gas is then filtered to remove oxygen carrier fines. The cleaned gas is conveyed to a gas-conditioning system for further filtration and residual water removal. The conditioned gas then follows to a multicomponent gas analyzer. The AR gas is sampled directly from the AR chimney and then undergoes the same treatment sequence as the FR flue gas, but without the first condenser step. A primary condenser is not required as the water content of AR gas is much lower than that of the FR. The gas analyzers, gas-conditioning systems, the gases measured, and the measurement uncertainties are summarized in Table 3.

3.5. Auxiliary reactor systems

All auxiliary reactor systems such as pressure and temperature measurement, flue gas filtration, the air preheater, reactor oven, and the data acquisition and control system have been adapted from the original 10 kW reactor by Lyngfelt and Berguerand. A new steam generator capable of precise control of the FR fluidization flow was custom built for the new reactor.

3.6. Oxygen carrier and fuel

The new 10 kW solid fuel CLC reactor was commissioned with ilmenite as the oxygen carrier. Ilmenite was chosen as it is the most tested oxygen carrier for solid fuel CLC and has been extensively used on the original 10 kW unit with petcoke and coal [19,25,26,28,37–39], and with biomass fuels [24]. Five different biomass fuels of different volatiles content and different alkali content were tested in the campaign. Table 4 summarizes the fuels used, their manufacturing and preparation processes, and the approximate fuel particle size. Composition of the fuels is summarized in Table 5.

4. Data evaluation

Reactor operational data were recorded throughout the experiments with a sampling rate of 1 Hz. To make data processing more manageable, the data was down-sampled to 0.167 Hz. This was deemed reasonable, since the performance parameters in question tend to respond to operational changes within tens of seconds, rather than seconds. Key operational parameters were calculated from the acquired data are discussed below.

5. Reactor total solids inventory

Reactor total solids inventory was calculated from the pressure measurements, making use of the fact that in fluidized conditions, pressure drop depends of the mass of fluidized material and the cross sectional area of the reactor section for which the pressure drop is measured. The reactor geometry was broken down into segments of constant cross sectional area and the inventory held in each section was calculated:

$$m_{oc,i} = \frac{A_i \Delta P_i}{g} \quad (1)$$

Here, $m_{oc,i}$ is the mass of OC held in section i of the reactor, ΔP_i is the pressure drop recorded over reactor section i, and g is the gravitational constant.

6. Circulation index

Circulation Index (CI) is a parameter that indicates the relative circulation rate of the reactor system. CI is calculated as a product of the AR riser pressure drop and the air flow rate of the AR.

Table 3
Gas composition analysis key equipment and measurement characteristics.

Analysis	Gas conditioning system	Gas analyzer	Measured components	Measurement principle	Measurement range	Measurement uncertainty
FR Flue Gas Composition	M&C Products SS-5	Rosemount NGA-2000 MLT4	CO	NDIR	0–100%	<2.0%
			CO_2	NDIR	0–100%	<2.0%
			CH_4	NDIR	0–100%	<2.0%
			H_2	TC	0–20%	<0.4%
			O_2	Paramagnetic	0–100%	<2.0%
AR Flue Gas Composition	M&C Products SS-5	SICK MAIHAK SIDOR	CO	NDIR	0–20%	<2.0%
			CO_2	NDIR	0–5%	<0.5%
			O_2	Paramagnetic	0–25%	<0.2%

Table Abbreviations: NDIR – non-dispersive infrared, TC – thermal conductivity.

Table 4
Manufacturing, preparation and average size of biomass fuels used in the campaign.

Fuel	Supplier	Manufacturing process	Additional fuel preparation	Approximate fuel particle size (as fed to the FR)
Black Pellets (BP)	Arbaflame AS, Norway	Stem wood is steam exploded, resulting pulp is pelletized	BP pellets are crushed to a size of 0.7–2.8 mm	Approximately 0.7–2.8 mm
Swedish Wood Char (SWC)	Skogens Kol AB, Sweden	Charring of stem wood to produce char particles of approximately 5 mm size	n/a	Fuel feed-screw reduces char size to approximately 0.8 mm
German Wood Char (GWC)	Holzkohleverarbeitung Schütte GmbH, Germany	Charring of stem wood, to produce char particles, sieved to approximately 0.25 mm size	n/a	Approximately 0.25 mm
Pine Forest Residue (PFR)	National Renewable Energy Centre (CENER), Spain	Palletization of pine wood chips	BP pellets are crushed to a size of 0.7–3.0 mm	Approximately 0.7–3.0 mm
Straw Pellet Mix (SPM)	CENER, Spain (for straw pellet component)	Palletization of wheat straw	Wheat straw pellets are crushed to a size of 0.7–3.5 mm, then mixed with crushed black pellets (50/50 wt%)	Approximately 0.7–3.5 mm

Table 5
Composition of biomass fuels used in the commissioning campaign.

Component	Unit (s)	Black pellets (BP)	Swedish wood char (SWC)	German wood char (GWC)	Pine forest residue (PFR)	Straw pellet mix (SPM)
Moisture	%	6.9	3.9	5.1	9.2	7.9
Ash, ar	%	0.3	5.5	2.8	1.8	4.1
Volatiles, ar	%	74.2	16.7	15.7	80.0	74.6
Fixed C, ar	%	18.7	73.9	76.4	9.0	13.5
C, ar	%	49.8	78.7	81.2	46.9	45.9
H, ar	%	5.6	3.3	3.0	5.7	5.8
N, ar	%	0.09	0.36	0.48	0.35	0.38
O, ar	%	37.4	12.1	12.5	36.0	40.2
S, ar	%	<0.012	0.03	0.018	0.04	0.108
Cl, ar	%	<0.01	<0.01	–	–	0.17
Si, ar	mg/kg fuel	<530	2068	12,000	–	9765
Ca, ar	mg/kg fuel	820	5895	12,000	–	4260
K, ar	mg/kg fuel	460	2585	4400	2080	5730
Na, ar	mg/kg fuel	<53	<270	<110	27	157
LHV, ar	MJ/kg fuel	18.64	29.838	30.03	17.97	16.85

$$CI = \Delta P_{AR\ riser}\dot{Q}_{AR\ air} \tag{2}$$

7. Carbon capture efficiency

Oxide oxygen efficiency is a measure of carbon capture efficiency and is defined as the ratio of the oxygen used for oxidation of the OC in the AR to the total oxygen consumed in the AR:

$$\eta_{oo}[\%] = 100^{*}\frac{0.2099 - (1+d)x_{O2,AR} - (1+d)x_{CO2,AR}}{0.2095 - (0.9996+d)x_{O2,AR} - 0.2095x_{CO2,AR}} \tag{3}$$

$$\text{Were, } d = \frac{\dot{Q}_{dilution\ N2}}{\dot{Q}_{air}} \tag{3.1}$$

Here d is the ratio of the dilution nitrogen flow introduced into the AR from the upper and lower loop seals, as well as pressure tap and fuel chute purge nitrogen introduced into the AR. Coefficients in Eq. (3) also account for the fact that air fed into the AR contains 400 ppm of CO_2.

8. Oxygen demand

Oxygen demand is the ratio of the oxygen required to fully oxidize the flue gas of the fuel reactor to the stoichiometric oxygen required for complete fuel oxidation. Oxygen demand is defined as:

$$\Omega_{OD}[\%] = 100^{*}\frac{0.5x_{CO,FR} + 2x_{CH_4,FR} + 0.5x_{H_2,FR}}{\Phi_o(x_{CO_2,FR} + x_{CO,FR} + x_{CH_4,FR})} \tag{4}$$

Here $\Phi_o$is the molar ratio [mol O2 required for combustion/kg fuel] / [mol C/kg fuel]. Gas conversion efficiency is then defined as:

$$\eta_{gas\ conv.}[\%] = 100 - \Omega_{OD} \tag{5}$$

It should be noted, that Ω_{OD} and $\eta_{gasconv.}$, do not account for the unconverted fuel that escapes with the fuel reactor flue gas as unconverted char. Higher order hydrocarbon species (C2, C3, etc.) are also not accounted for, but have been shown from previous CLC operation to be minimal.

9. Alkali emissions

Determination of the raw flue gas alkali concentration requires processing of the SID signal and correction of the diluted measurement to undiluted basis. SID signal processing involves averaging the signal with a 10 s running average to minimize signal noise. For FR sampling, the sample dilution ratio is calculated with Eq. (6).

$$DR_{FR} = \frac{CO_{2\ FR\ undiluted(dry\ basis)}}{CO_{2\ FR\ diluted\ (dry\ basis)}} \tag{6}$$

Here, the undiluted CO_2 concertation is reported by the main process gas analyzer, and the diluted CO_2 concentration is reported by an independent CO_2 analyzer that is a part of the alkali measurement setup. For AR sampling, a similar approach is used, but O_2 is used as the tracer gas. The AR sample dilution ratio is calculated as per Eq. (6) but using the undiluted and diluted O_2 concentrations. The undiluted O_2 concentration is reported by main process gas analyzer, and the diluted O_2 concentration is reported by an independent trace oxygen analyzer that is a part of the alkali measurement setup. Once the dilution ratio is determined, the raw flue gas is calculated as a product of the SID signal value, the dilution ratio, and the SID calibration constant. The resulting values are expressed in units of mg K/m^3_{normal}. After calculation, the resulting raw flue gas alkali concentrations were reviewed to reject erroneous data that occurs due to upset conditions that include cleaning of the main gas analysis system, sampling probe plugging, and sampling probe purging.

10. Oxygen carrier alkali absorption

Since sodium levels of the fuels used in the campaign are insignificant when compared to the potassium content, the oxygen carrier alkali

Table 6
New 10 kW_{th} CLC pilot system operational results summary.

Day	Fuel	Test Duration	Sub-Test	Test Type	Reactor OC Inventory (kg)	FR Temperature (°C)	Fuel Feed Rate (kg/hr)	P_{fuel} (kW)	FR OC Inventory (kg)	CI/P_{fuel} (kPa nL/min kW)	η_{oo} (%)	Ω_{OD} (%)	$\eta_{gas\ conv.}$ (%)
Day 1	GWC	00:18:00	GWC 1		22.8	957	0.83	6.9	12.1	73.4	68.2	15.1	84.9
			GWC 2		22.5	968	0.83	6.9	12.7	26.6	91.7	9.5	90.5
	BP	00:54:00	BP 1		22.1	970	1.26	6.5	12.9	22.7	99.0	31.7	68.3
			BP 2		21.3	972	1.26	6.5	12.8	11.8	99.5	33.2	66.8
		02:40:00	BP 3		23.6	978	1.26	6.5	13.0	36.5	99.6	29.9	70.1
			BP 4		23.2	972	1.26	6.5	12.8	21.2	98.2	31.3	68.7
			BP 5		21.3	971	1.26	6.5	12.3	5.4	99.9	49.6	50.4
			BP 6		20.1	968	1.26	6.5	12.1	3.1	99.3	62.7	37.3
			BP 7		23.6	975	1.26	6.5	12.9	18.7	98.9	35.9	64.1
Day 2	SWC	01:46:00	SWC 1	BT	24.9	983	0.69	5.7	12.2	43.6	92.7	6.1	93.9
			SWC 2	BT	25.1	988	0.69	5.7	12.4	72.6	94.7	5.3	94.7
			SWC 3	BT	25.0	987	0.69	5.7	12.1	30.0	95.2	4.9	95.1
			SWC 4	BT	25.0	986	0.69	5.7	11.9	16.0	96.4	5.5	94.5
			SWC 5		24.8	987	0.69	5.7	11.6	4.4	97.2	10.1	89.9
Day 3	BP	02:56:00	BP 8	BT	43.1	975	1.2	6.2	12.5	76.3	99.1	22.2	77.8
			BP 9	BT	41.5	977	1.2	6.2	12.2	49.5	98.7	21.8	78.2
			BP 10	BT	42.6	971	1.2	6.2	12.2	99.0	97.8	21.9	78.1
	PFR	00:54:00	PFR 1	BT	39.1	977	1.08	5.3	11.9	14.6	97.1	24.4	75.6
			PFR 2	BT	41.3	979	1.08	5.3	12.3	73.6	99.3	23.7	76.3
Day 4	BP	00:49:00	BP 11	BT	39.8	986	1.17	6.1	12.6	164.6	100.0	19.9	80.1
			BP 12	BT	37.2	991	1.75	9.1	12.2	85.8	100.0	20.4	79.6
		00:46:00	BP 13	BT	32.0	992	1.75	9.1	12.2	50.5	99.8	22.8	77.2
			BP 14		26.2	986	2.34	12.1	11.4	14.5	99.8	30.7	69.3
		01:24:00	BP 15		34.3	977	1.75	9.1	12.7	87.1	100.0	26.7	73.3
			BP 16		31.8	975	1.75	9.1	12.2	27.8	99.6	28.3	71.7
			BP 17		30.7	979	2.34	12.1	12.2	27.3	92.9	30.3	69.7
			BP 18		26.0	955	1.75	9.1	11.7	8.7	100.0	36.0	64.0
			BP 19		24.4	936	1.75	9.1	11.3	12.8	98.6	42.8	57.2
Day 5	BP	02:44:00	BP 20		35.5	885	1.75	9.1	12.4	51.4	94.6	28.5	71.5
			BP 21		33.3	879	1.95	10.1	12.2	37.9	93.6	30.6	69.4
			BP 22		36.1	879	1.95	10.1	12.1	33.7	90.7	32.3	67.7
			BP 23		33.2	898	2.14	11.1	11.7	23.0	96.0	35.8	64.2
	PFR	01:16:00	PFR 3	BT	34.5	924	1.53	7.5	12.1	44.7	99.4	24.7	75.3
			PFR 4		34.1	925	1.67	8.2	11.8	44.7	99.4	25.4	74.6
			PFR 5		33.5	922	1.95	9.6	11.3	6.8	99.6	36.2	63.8
Day 6	SPM	03:20:00	SPM 1	BT	36.4	898	1.52	7.2	11.9	55.0	94.2	25.2	74.8
			SPM 2	BT	34.5	922	1.52	7.2	11.3	17.0	98.1	25.0	75.0
			SPM 3		34.1	921	1.52	7.2	10.8	8.6	98.9	30.8	69.2
			SPM 4		33.2	921	1.52	7.2	10.6	3.8	98.1	50.8	49.2
			SPM 5		32.4	921	1.52	7.2	10.7	4.1	97.3	49.2	50.8

Table Abbreviations: GWC – German wood char, BP – black pellets, SWC – Swedish wood char, PFR – pine forest residue, SPM – straw pellet mix, BT – benchmarking test.

absorption can be estimated based on the concentration of K in the bed material:

$$OC\ Alkali\ Absorbtion[\%] = 100*\frac{K_{accum.\ by\ OC}}{K_{input\ by\ fuel}} \quad (7)$$

In Eq. (7), input of K by the fuel, $K_{inputbyfuel}$, is calculated as the product of the fuel feed rate and the concentration of potassium in the fuel (as determined from the fuel's composition). The accumulation of K in the OC, $K_{accum.byOC}$, is determined as the product of the system's OC inventory and the difference in K concentration in the OC before and after a test period.

11. Results

Commissioning of the new 10 kW solid fuels CLC reactor spanned six days with over 21 h of fueled operation achieved. Five different fuels were used with fuel feed rates ranging from 0.7 to 2.3 kg/hr, which corresponds to thermal power rates ranging from 5.3 to 12.1 kW_{th}. A summary of operational results is presented in Table 6 below.

In Table 6, tests are defined as continuous operation of a given test fuel started from hot circulating conditions. Test duration is reported for the entire fuel feeding period. Subtests are denoted with the acronym of the fuel as well as the sub-test sequence number. Each of the sub-tests represents a subset of uninterrupted operation with a set fuel feed rate and AR air flow rate. The data reported for the sub-tests represents averages taken from steady operating periods. These periods were selected to exclude the transient behavior at initiation of fuel feeding. Additionally, periods where experimental data collection was interrupted by mitigation of operational issues (e.g. online cleaning of the gas conditioning systems) were also excluded. Several of the sub-tests were conducted in order to study the response of operating parameters on system performance. In some tests, the fuel feed rate was deliberately raised, or the AR flow rate was deliberately lowered, to explore the onset of gasification conditions. Tests where steady chemical looping combustion was established are classified as benchmarking tests (BT). Results from these tests are especially useful as performance benchmarks for future test campaigns.

It should be noted that within this commissioning campaign, significant operational upsets were experienced during two tests with SWC and GWC fuels due to excessive backpressure in the FR chimney. It was found that the backpressure was caused by unconverted wood char being carried into the FR chimney and setting on the chimney walls. Significant amounts of wood char were found in the FR water seal and in the material removed during subsequent FR chimney cleaning. Wood char was also found in the AR filters, confirming that once significant back pressure developed in the FR chimney, disbalance in pressure between the AR and FR caused one or both of the loop seals to blow out, allowing char to be carried over into the AR and then to the AR chimney and AR filters. Results from these tests were omitted.

AR and FR flue gas alkali measurement was conducted throughout the commissioning campaign. Collection of alkali measurements proved to be challenging primarily due to the difficulty of maintaining a stable sampling dilution ratio. When sampling, the dilution ratio was manipulated by setting the 1st and 2nd stage dilution nitrogen flow. The dilution at the third stage diluter was fixed at 8:1. The stability of the overall dilution ratio was monitored from the trace CO_2 (when sampling the FR) and trace O_2 measurements (when sampling the AR) of the diluted sample. During measurement, the trace CO_2 and O_2 measurements declined over time, indicating that the raw sample suction flow was decreasing. The likely cause of this was gradual plugging of the sampling probes with the OC fines present in the exhaust flow. This issue was mitigated by periodically backflushing the probes with nitrogen. This method proved to be effective, but temporarily affected the alkali data collection. During data processing, alkali measurements affected by probe back flushing and cleaning of the main gas analyzer system were mostly excluded. Alkali measurement results are presented in Table 7.

Table 7
New 10 kW_{th} CLC pilot system alkali measurement results.

Sub-Test	Concentration Basis		Mass Flow Rate Basis			Relative Mass Basis		
	FR Alkali (μg K/nm^3_dry)	AR Alkali (μg K/nm^3_dry)	Alkali Feed (mg K /min)	FR Alkali (mg K/min)	AR Alkali (mg K/min)	FR % Release	AR % Release	Bed % Retention
BP 1	5817	–	10.8	0.16	–	1.47%	–	–
BP 2	7034	–	10.8	0.22	–	2.04%	–	–
BP 3	6632	–	10.8	0.20	–	1.86%	–	–
BP 4	7265	–	10.8	0.22	–	2.04%	–	–
BP 5	5585	–	10.8	0.18	–	1.66%	–	–
BP 6	4563	–	10.8	0.15	–	1.40%	–	–
BP 7	6063	–	10.8	0.19	–	1.78%	–	–
BP 8	6760	742	10.3	0.20	0.15	1.99%	1.45%	96.56%
BP 9	5337	461	10.3	0.16	0.09	1.56%	0.90%	97.54%
BP 10	5943	1155	10.2	0.18	0.25	1.79%	2.49%	95.73%
BP 11	3578	–	10.0	0.12	–	1.16%	–	–
BP 12	7646	–	15.0	0.24	–	1.63%	–	–
BP 13	8361	609	15.0	0.32	0.12	2.11%	0.80%	97.09%
BP 14	7623	–	20.0	0.34	–	1.71%	–	–
BP 15	9004	–	15.0	0.33	–	2.21%	–	–
BP 16	7242	1088	15.0	0.27	0.19	1.79%	1.30%	96.91%
BP 17	–	1087	20.0	–	0.21	–	1.07%	–
BP 18	6082	1616	15.0	0.23	0.33	1.51%	2.17%	96.32%
BP 19	4048	–	15.0	0.14	–	0.95%	–	–
PFR 1	8230	–	37.9	0.26	–	0.67%	–	–
PFR 2	–	1042	37.9	–	0.23	–	0.60%	–
SWC 1	13,394	–	32.8	0.37	–	1.13%	–	–
SWC 4	18,509	–	32.8	0.48	–	1.45%	–	–
SWC 5	13,908	–	32.8	0.36	–	1.10%	–	–
SPM 1	22,510	1589	149.1	0.73	0.28	0.49%	0.19%	99.32%
SPM 2	37,791	–	149.1	1.24	–	0.83%	–	–
SPM 3	48,956	461	149.1	1.58	0.06	1.06%	0.04%	98.90%
SPM 4	20,385	540	149.1	0.67	0.07	0.45%	0.05%	99.50%
SPM 5	25,490	1102	149.1	0.70	0.14	0.47%	0.10%	99.43%

Table Abbreviations: GWC – German wood char, BP – black pellets, SWC – Swedish wood char, PFR – pine forest residue, SPM – straw pellet mix, BT – benchmarking test.

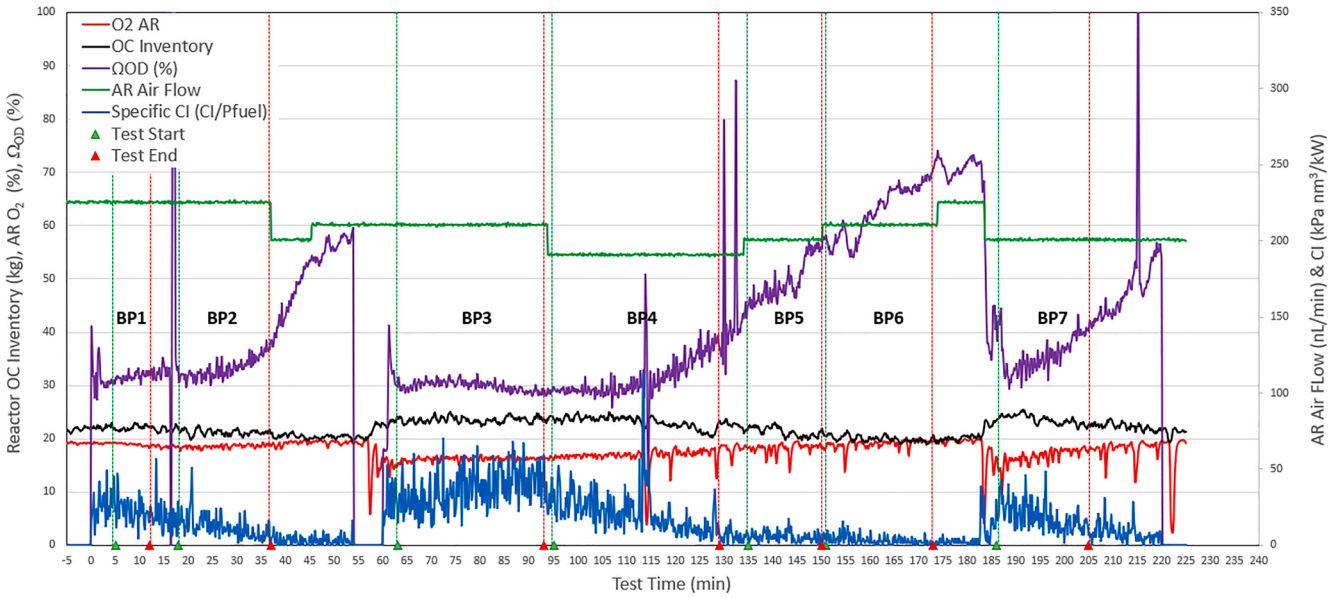

Fig. 5. Selected operational and performance parameters for sub-tests BP 1 to BP 7. *Dashed lines show start (green) and end (red) times for the presented sub-tests.* (For interpretation of the references to colour in this figure legend, the reader is referred to the web version of this article.)

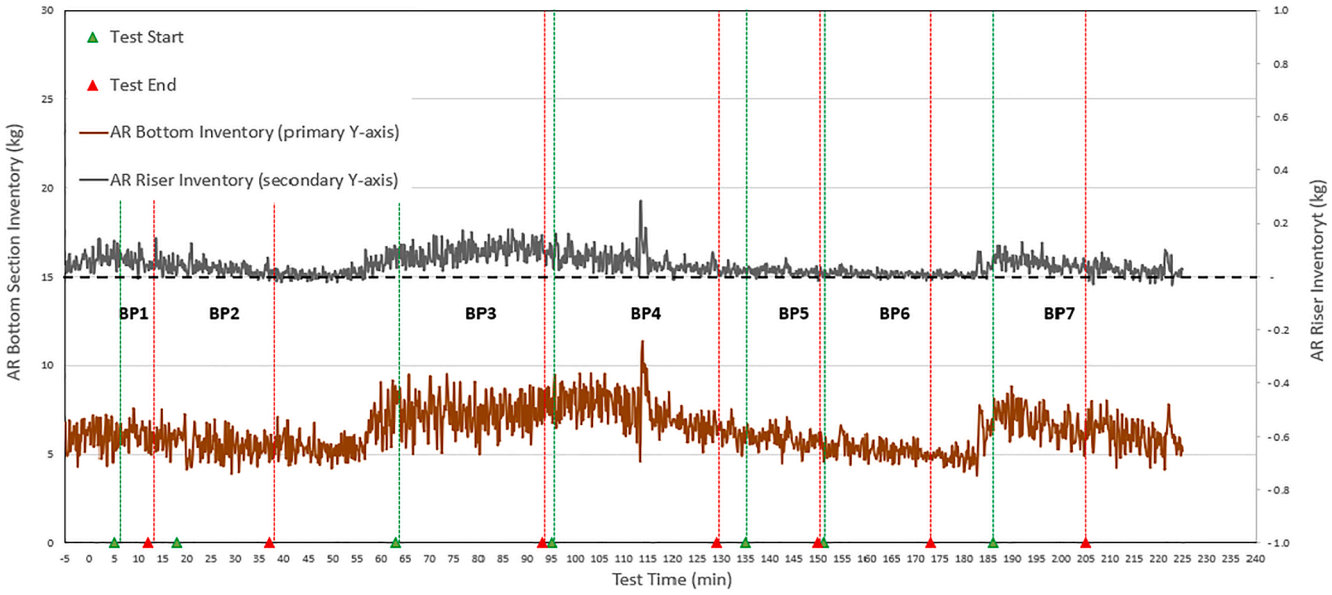

Fig. 6. AR solids inventory levels for sub-tests BP 1 to BP 7. *Dashed lines show start (green) and end (red) times for the presented sub-tests.* (For interpretation of the references to colour in this figure legend, the reader is referred to the web version of this article.)

12. Discussion

12.1. Reactor performance

The first operational learning for the new 10 kW reactor was established during initial tests with BP fuel. Fig. 5 shows selected operating and performance parameters for sub-tests BP 1 through BP 7. These tests indicate that a minimum system OC inventory of approx. 22 kg of OC is required before effective circulation of the system can be achieved. The lack of inventory was evident from the fact that oxygen demand for black pellets is high and increases as reactor inventory decreases. This indicates that delivery of oxygen in the form of oxidized OC circulated to the FR is quite low. When fresh material is added to the FR, at 56 min and 183 min, a step decrease in oxygen demand is observed, indicating the onset of effective circulation of oxidized OC into the FR. This is corroborated by the O_2 concentration of the AR. AR O_2 levels are generally high, indicating that very little reduced OC is overflowing from the FR. When inventory is topped off, the AR O_2 concentration drops, increased transfer of reduced OC to the AR.

Fig. 6 shows the inventory levels of the AR bottom section and the AR riser for the tests. The figure clearly shows that the AR bottom section needs to accumulate more than approx. 5 kg of ilmenite, prior to any significant level of inventory appearing in the AR riser section. The onset of inventory in the AR riser signifies the onset of effective global OC circulation within the system.

Gas composition in the FR for the same set of sub-tests is shown in Fig. 7.

In Fig. 7, the effect of insufficient circulation to the FR can be clearly seen as CO and H_2 levels increase and CO_2 levels fall in periods corresponding to a decrease in system inventory. These conditions have a

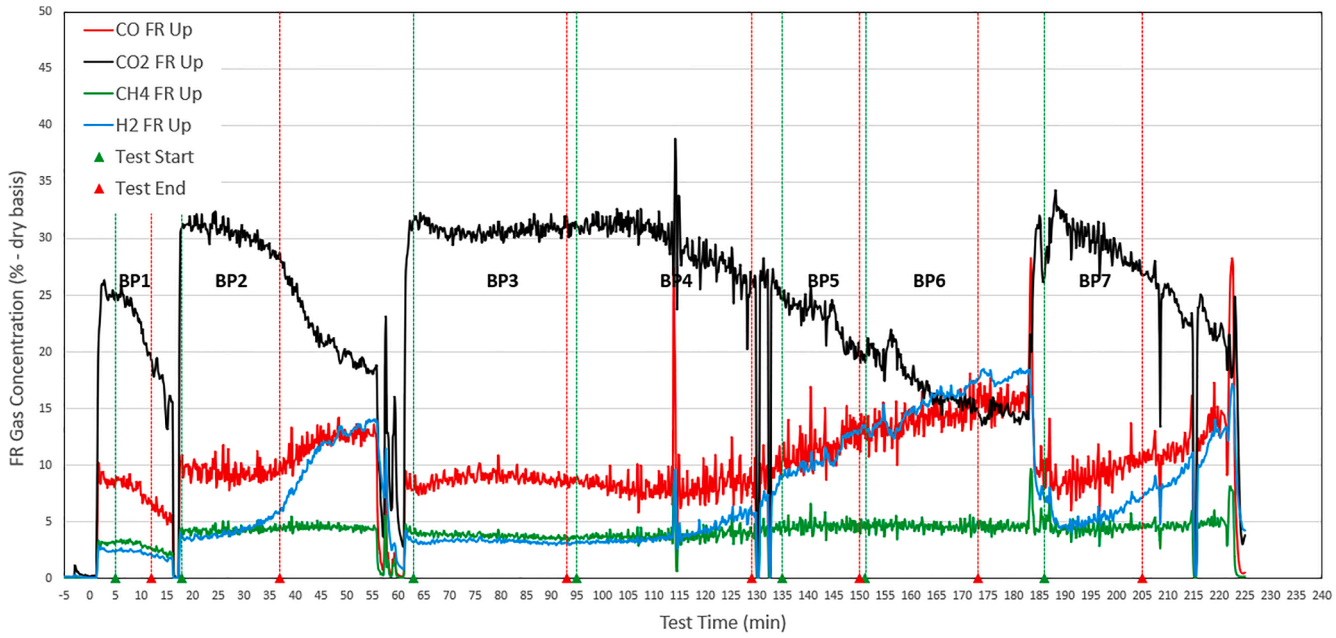

Fig. 7. FR gas composition for sub-tests BP 1 to BP 7. *Dashed lines show start (green) and end (red) times for the presented sub-tests.* (For interpretation of the references to colour in this figure legend, the reader is referred to the web version of this article.)

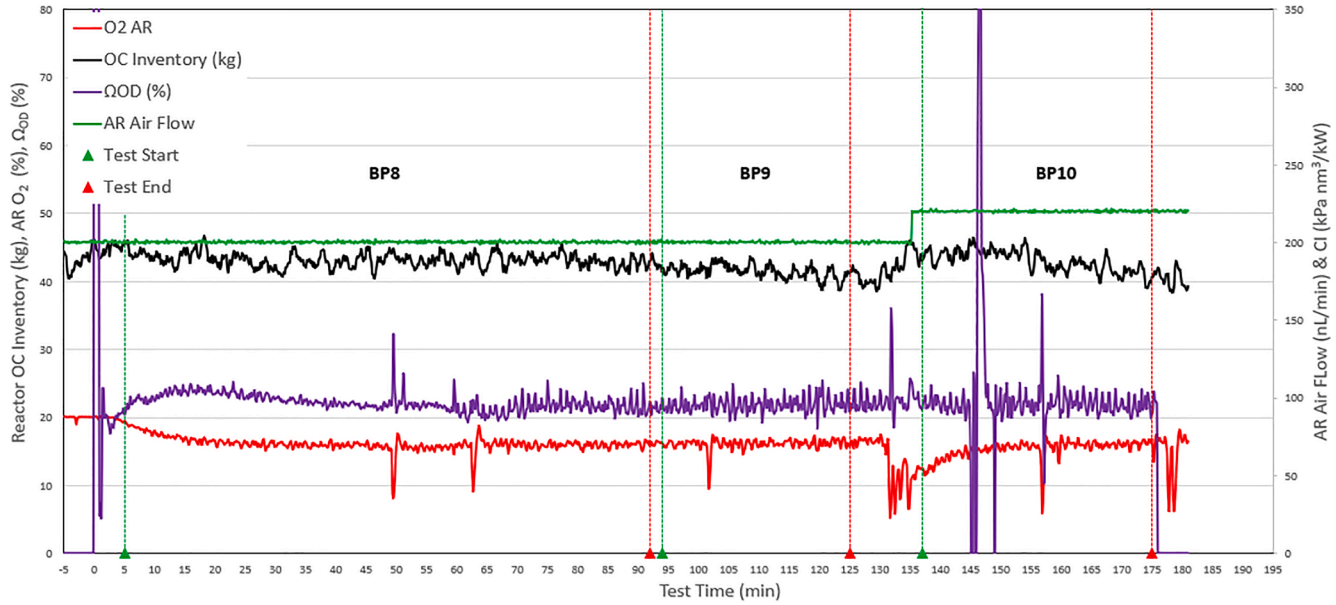

Fig. 8. Selected operational and performance parameters for sub-tests BP 8 to BP 10. *Dashed lines show start (green) and end (red) times for the presented sub-tests.* (For interpretation of the references to colour in this figure legend, the reader is referred to the web version of this article.)

closer resemblance to chemical looping gasification (CLG).

In light of establishing minimum effective inventory for the new 10 kW CLC system, tests for the remainder of the commissioning campaign were performed at inventory levels of above 22 kg, maintaining levels above 5 kg of ilmenite in the AR's bottom section. This proved to be a difficult task, as elutriation of bed material from the FR to the FR chimney was significant. For example, it was found that during the first campaign day, which included almost 4 h of fueled operation and approximately 1.5 h of unfueled circulation in hot conditions, 5.1 kg of OC material were carried over and settled in the FR chimney and the FR water seal. This level of elutriation was observed for the remainder of the campaign.

The effect of increased overall inventory, and thus the AR inventory, can be seen in Figs. 8 and 9 for sub-tests BP 8 to BP 10. Here the total inventory level is maintained at a level close to 40 kg, with the AR holding approximately 24 to 26 kg of ilmenite in the bottom section and FR holding approximately 14 to 16 kg of ilmenite. The oxygen demand is around 20 to 25%, indicating effective delivery of oxidized OC to the FR for fuel conversion. This is confirmed by a much higher proportion of CO_2 vs CO in the FR and a level of H_2 below 2%.

From the tests summarized in Table 6, several subtests were conducted specifically for establishing benchmark performance data for this new reactor. These were designated as benchmarking tests (BT). A summary of benchmarking test results is presented in Table 8. It should be noted that no performance benchmark data is presented for GWC fuel. Tests with GWC fuel were short, and stable system operation was

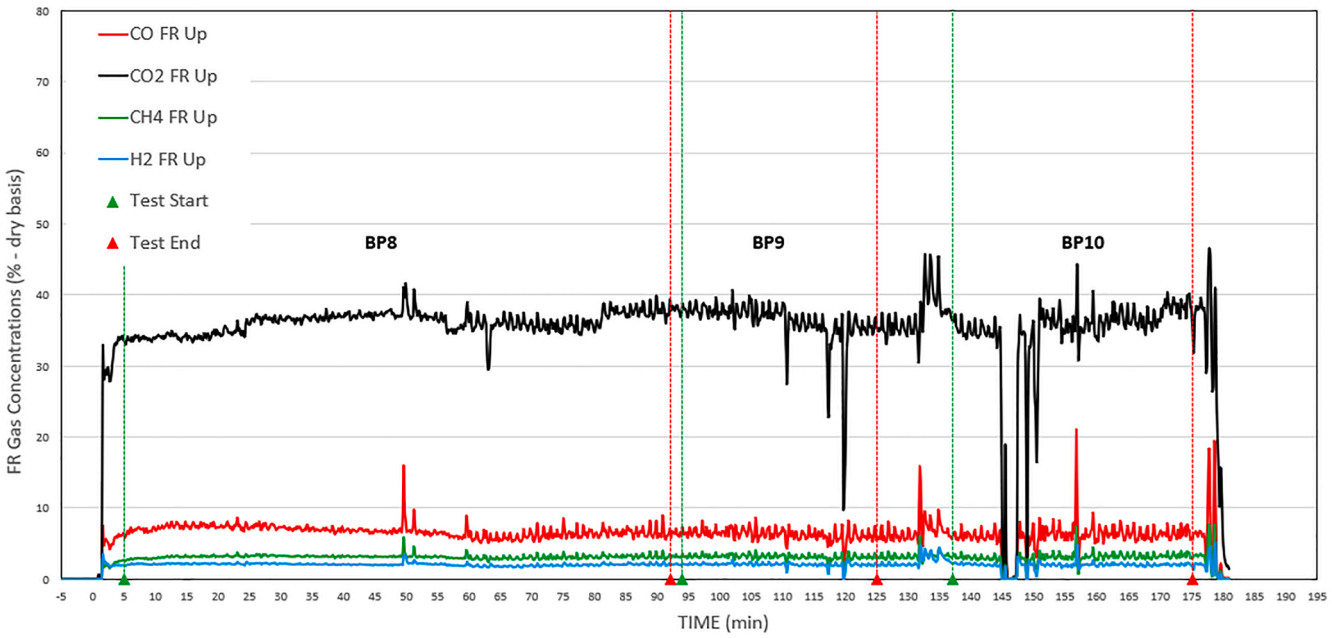

Fig. 9. FR gas composition for sub-tests BP 8 to BP 10. *Dashed lines show start (green) and end (red) times for the presented sub-tests.* (For interpretation of the references to colour in this figure legend, the reader is referred to the web version of this article.)

Table 8
Summary of the new 10 kW_{th} CLC system benchmarking tests.

Fuel	Reactor OC Inventory (kg)	FR Temp. (°C)	Fuel Feed Rate (kg/hr)	P_{fuel} (kW)	$CI_{specific}$	η_{oo} (%)	Ω_{OD} (%)	$\eta_{gas\ conv.}$ (%)
BP	39.4	982.1	1.4	7.1	87.6	99.2	21.5	78.5
SWC	25.0	986.1	0.7	5.7	40.5	94.8	5.5	94.5
PFR	38.3	960.0	1.2	6.0	44.3	98.6	24.3	75.7
SPM	35.4	909.6	1.5	7.2	36.0	96.1	25.1	74.9

Table 9
Carbon capture efficiency of the old 10 kW CLC pilot system.

	Fuel\OC	Mn Ore (Sibelco)	Steel Converter Slag	Mn-Si-Ti	Mn Ore (SinFin)	Mn Ore (Mangagran)	Mn Ore (Mesa)
η_{oo} (%)	BP	98–99	87–99.9	–	–	n/a	n/a
	GWC	96–98	–	–	–	n/a	n/a
	SWC	78–93	83–98	81–95	66.5–95.6	82.4–96.4	76.0–83.9
Reference ►		[31]	[32]	[30]	[29]	[29]	[29]

Table 10
Oxygen demand for various fuels and oxygen carriers in the 10 and 100 kW Units. (See above-mentioned references for further information.)

			OC ↘	NEW 10 kW	10 kW				100 kW			
Increasing Oxygen Demand ↓	Fuel	Volatiles Content (wt%)		Ilmenite	Ilmenite	SinFin Mn Ore	MnSiTi	Sibelco Calcined Mn Ore	Ilmenite	Ilmenite + Brazilian Mn Ore	Sinaus Mn Ore	Sibelco Calcined Mn Ore
	SWC	17		4.9%		5.0%		6.0%			6.0%	6.0%
	GWC	16					3.8%	13.0%			10.3%	10.0%
	Petcoke	10			18.0%	12.0%	5.4%			8.0%	10.6%	
	Heat-treated Columbian Coal	29					10.1%					
	Columbian Coal	29							16.0%		11.7%	13.0%
	Lignite	45					20.0%					
	BP	74		21.8%				32.0%				22.0%
	Wood pellets	74								23.0%	25.0%	
Reference ►					[28]	[28]	[28]	[31]	[41]	[42]	[43][44]	[31]

Note: Green arrows denote comparison of Mn ore performance vs. Ilmenite for a given reactor system. Red arrows denote comparison of reactors systems performance for a given oxygen carrier.

not achieved. For these reasons the results for the GWC fuel were deemed to be suboptimal, and not an appropriate for benchmarking the reactor performance.

Results presented in Table 8 indicate that carbon capture efficiency achieved is > 99% for black pellets, >98 for pine forest residue, >96% for straw pellets, and > 94% for Swedish wood char. Although, not included in the benchmarking data, German wood char operation had carbon efficiencies of 68.2 and 91.7%. The lower carbon capture efficiency of the char fuels can be explained by the fact that the wood chars have non-volatile fraction of approx. 85%, vs. the 15–20% non-volatile content of straw, black pellets, and pine forest residue fuels. The higher char fraction increases the probability of unconverted char carry-over to the AR. Char that makes into the AR, readily burns in the presence of air, lowering the carbon capture efficiency of the system.

Average reported values of η_{oo} for the previous generation 10 kW solid fuel CLC pilot are summarized in Table 9. Although no operation with ilmenite and biomass fuel is reported for the older generation reactor, the oxygen carriers in Table 9 have been previously shown to generally yield similar carbon capture efficiency compared to ilmenite. As such, comparison of the new reactor's performance to that of the old unit is relevant.

The previous generation 10 kW solid fuels reactor was equipped with a carbon stripper designed to recirculate char at the FR outlet back to the FR inlet. The carbon stripper was meant to increase the char's residence time in the FR and improve its conversion, thus decreasing char breakthrough to the AR [40]. As summarized in Table 9, carbon capture efficiency of the previous generation unit was reported in the range of 96–99 % for German wood char [31], 76–97% for Swedish wood char [29–32], and 87–100% for black pellets [31,32]. The current unit was designed without a carbon stripper but was able to achieve carbon capture efficiencies like those of the previous unit, thus suggesting that high carbon capture efficiency is achievable without the need for a carbon stripper, when the reactor is operated with biomass fuels. However, the case may be different for solid fossil-derived fuels such as coal and petcoke. Fossil-derived solid fuel char is well-known to be less reactive than biomass char [15].

The oxygen demand demonstrated by the new system ranges from 4.9 to 25.5%. Here, the main difference in oxygen demand is again related to the fuel's composition. For straw, black pellets, and pine forest residue, up to 75% of the fuel mass, the volatiles fraction, is quickly devolatilized. This fast release limits the contact time between the volatiles and the OC in the FR bed, resulting in only partial conversion of the volatiles. For the char fuels, release of most of the fuel's combustible content is limited by the char gasification rate, giving time for the fuel particles to mix well with the bed material. Thus, the gradual release of the gasification products results in better contact between the reactive gaseous species and the OC particles, enabling higher gas conversion efficiency.

Table 10 compares the oxygen demand of the new 10 kW unit to the best results obtained with various fuels and oxygen carriers in the original 10 kW solid fuels unit and the larger 100 kW solid fuels unit.

In Table 10, fuels are ordered top to bottom in order of increasing oxygen demand. Each fuel's volatiles content is also reported. The operational data presented in Table 10 clearly shows a dramatic rise in oxygen demand with increasing volatiles content. There are two deviations to this trend. The largest one is that petcoke, despite having lower volatiles content, has a higher oxygen demand than SWC and GWC fuels. The explanation for this deviation can likely be related to fuel reactivities. Oxygen demand is essentially the degree of incomplete oxidation of the reactive gases released in fuel conversion. These gases consist of the fuel's volatiles and the syngas released from fuel char gasification. It is well known that volatile species are a lot less reactive than syngas. As such, reactive gasses with a higher volatiles-to-syngas ratio are less reactive and yield a higher oxygen demand. Petcoke char is known to be a lot less reactive than the biochar found in SWC and GWC fuels, resulting in a large proportion of the char leaving the FR unconverted. The reactive gases released in petcoke conversion are likely very rich in volatiles and result in an overall higher oxygen demand vs. the reactive gases higher in syngas proportion released in SWC and GWC fuel conversion. Furthermore, the volatile species found in biomass fuels are potentially more reactive than those in fossil-based fuels such as petcoke. The second deviation to the overall trend is that SWC performs slightly better than GWC, despite a lower volatiles content. This could be explained by the smaller particle size of the SWC fuel used in those studies. This effect was clearly shown when particle size of GWC fuel was varied [43].

Another trend noticeable from the presented data is that oxygen demands are generally lower for manganese ores as compared to ilmenite. This is evident from comparing the oxygen demand of Columbian Coal with Ilmenite relative to two Mn ores in 100 kW unit and comparing the oxygen demand of petcoke with Ilmenite to that of the Sinfin Mn ore in the 10 kW unit. Finally, the presented data also suggests that results from the 100 kW unit generally give lower oxygen demand. This is seen comparing BP and GWC fuels using Sibelco Calcined Mn ore.

From the observations that 1) Mn ore generally outperforms

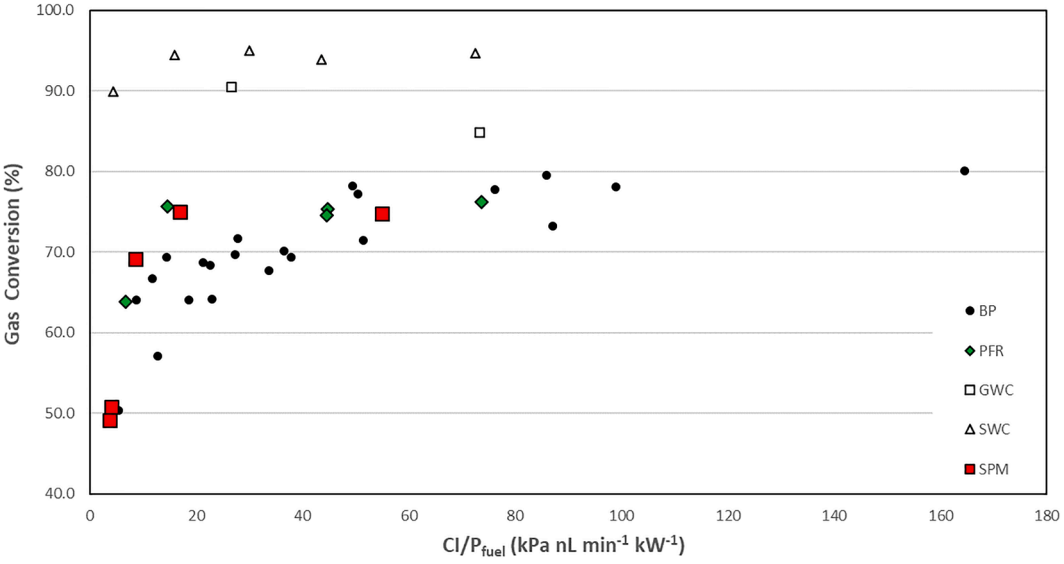

Fig. 10. Gas conversion efficiency vs. power-specific circulation index.

Ilmenite, and 2) the 100 kW unit generally outperforms the old 10 kW unit in terms of oxygen demand, we can conclude that the oxygen demand for ilmenite with BP fuel in the new 10 kW unit should be:

- higher than 32% - number obtained for black pellets and Mn ore in the original 10 kW unit
- significantly higher than 22% - the number obtained for Mn ore in the 100 kW unit
- likely significantly higher than 23 and 25% - oxygen demand reported for wood pellets in the 100 kW unit (black pellets and wood pellets are similar in composition and though to be comparable fuels)

The average demand of 21.5% reported for the new 10 KW leads to a conclusion that the new 10 kW shows a significant performance improvement over the previous version of the 10 kW CLC pilot. This improvement can likely be attributed to the use of the volatiles distributor, but unfortunately could not be directly evaluated in this study.

Further to capturing the general performance level of the new 10 kW CLC pilot, the influence of OC circulation was investigated. From the first tests conducted in this study, it was already established that OC circulation only starts to develop when the AR bottom section inventory exceeds approximately 5 kg. Higher circulation can be achieved with further inventory increase or with higher AR air flow rate. The effect of circulation on conversion is captured in Fig. 10, where gas conversion efficiency is plotted against specific circulation index (circulation index divided by fuel input power).

For the high-volatiles fuels, Fig. 10 shows that higher circulation (CI/P_{fuel}) results in higher gas conversion efficiency. There are several reasons for this. First, higher circulation simply increases the relative amount of oxygen input available for contact with the gaseous components of the fuel. Secondly, higher OC circulation results in lower OC conversion, which has two beneficial effects on fuel conversion. The kinetics of ilmenite reduction (fuel conversion) are known to be faster at low OC conversions. Also, since the overall FR process is endothermic, lower ilmenite conversion limits temperature decrease in the FR, keeping reaction kinetics fast [45].

It is worth noting that the data points for the two char fuels show an overall higher gas conversion efficiency vs. volatile fuels and lower dependency on the OC circulation rate. This can be explained by the fact that reactive gases released in conversion of the SWC and GWC fuels are composed mostly of highly-reactive syngas, the product of char gasification. For the high-volatiles fuels (BP, PFR, SPM) the reactive gases are dominated by less reactive volatile species. Furthermore, the release of the syngas from the SWC and GWC fuels is gasification-controlled, and thus more gradual than the fast release of volatiles of the high-volatiles fuels. The gradual release of syngas results in better contact with the oxygen carrier than can be expected to occur between the volatiles and the oxygen carrier.

Table 11
Summary of alkali release distribution.

Sub-Test	Mass flow rate basis			Relative mass basis		
	Alkali feed (mg/min)	FR alkali (mg K/min)	AR alkali (mg K/min)	FR % release	AR % release	Bed % retention
BP	12.9	0.21	0.19	1.70%	1.45%	96.8%
PFR	37.9	0.26	0.23	0.67%	0.60%	98.7%
SWC	32.8	0.40	–	1.23%	–	–
SPM	149.1	0.98	0.14	0.66%	0.09%	99.2%

12.2. Alkali emissions

Alkali emissions measurement proved to be quite challenging due to

Table 12
OC alkali retention determined from OC solids samples (last campaign day).

Fuel	Fuel feed rate (kg/hr)	Fuel feed duration (min)	Fuel potassium content (μg K/kg fuel)	Mass of potassium introduced (g K)
SPM	1.52	200	5730	29.0
GWC	2.28	62	4400	10.4
Total Potassium Input with Fuel (g K)				39.4
Average System Inventory Between Samples (kg)				34
OC Potassium Content Before Test (mg K/kg ilmenite)				860
OC Potassium Content After Test (mg K/kg ilmenite)				2000
Total Potassium Absorbed by OC (g K)				38.76
OC Alkali Absorption (%)				98.4%

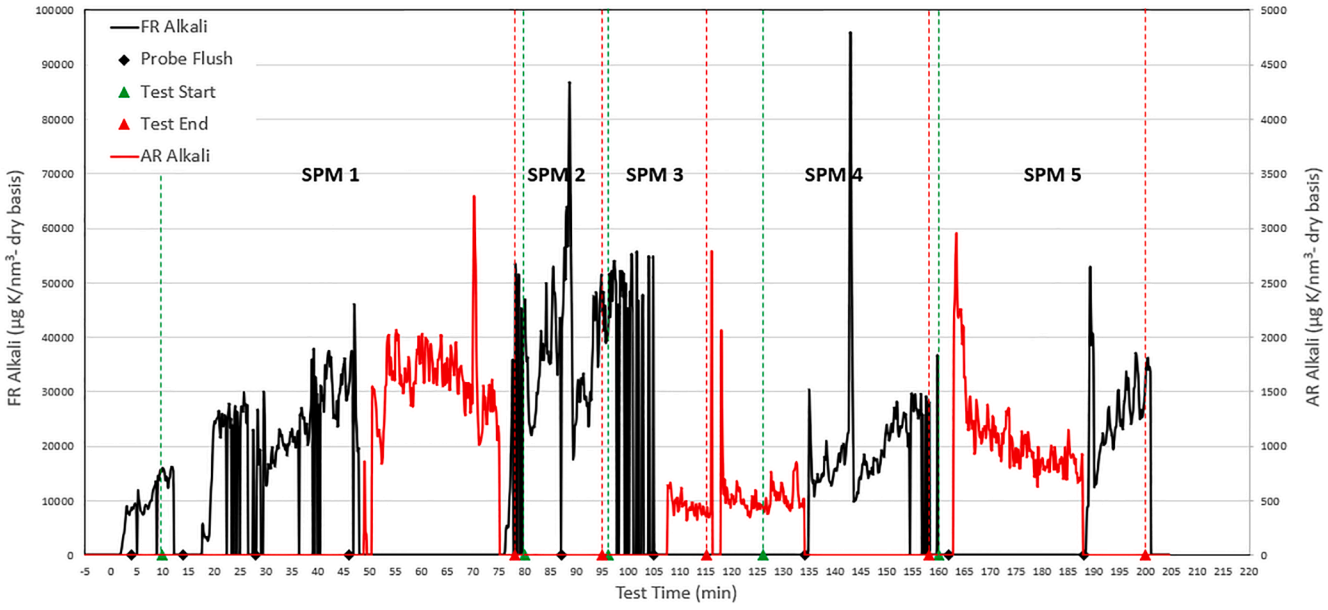

Fig. 11. AR and FR alkali emissions for sub-tests SPM 1 to SPM 5. *Dashed lines show start (green) and end (red) times for the presented sub-tests.* (For interpretation of the references to colour in this figure legend, the reader is referred to the web version of this article.)

instability of sampling that was suspected to occur due to ingress of solid particles into the alkali sampling probe during testing. Fig. 11 shows SID alkali measurements for the SPM fuel tests. The extreme peaks in the signal correspond to a manual change in dilution settings. The missing data is a result of rejecting data in the data processing stage due to measurement instability.

The collected alkali emissions data set presented in Table 7 represents the most comprehensive survey of alkali emissions in CLC at the time of publication. The only other previously reported results were conducted in an earlier study performed on the Chalmers 100 kW CLC pilot system [24], but presented very limited data on the alkali release levels of the AR. This was largely due to the inability to accurately track AR sample dilution during measurement. Since this earlier study, the measurement methodology was enhanced with the ability to track AR sample dilution through measurement of raw and diluted O_2 concentration of the AR sample. This improvement was implemented in this study and represents a significant step forward with respect to AR alkali measurement validity. To make the discussion of the alkali results easier, Table 11 shows a summary of the average alkali results.

Table 11 reveals a few trends. Increase of the fuel's alkali content seems to result in higher alkali release in the FR. This effect, however, is not strictly proportional. For example, a 11-fold increase of alkali input that comes from switching fuel from BP to SPM, results in only a 5-fold increase in FR alkali emissions. Surprisingly, increase in alkali input rates, seems to have little to no effect on the AR alkali emissions levels. In fact, AR alkali emission of BP, PFR and SPM fuels are roughly equivalent despite the progressively higher alkali content of these fuels.

On a relative basis, for all fuels, experimental data shows that over 97% of the alkali introduced into the reactor with the fuels, are retained in the reactor system. It is expected that the majority of this retention can be attributed to retention by the bed material, as ilmenite is well-known to be effective at absorbing alkali thorough formation of alkali titanates [23,23]. This is consistent with the 98% retention rate reported for the 100 kW CLC unit when operated with a mixture of synthetic perovskite and ilmenite as the oxygen carrier [24]. To confirm alkali retention by Ilmenite, the OC alkali retention was also calculated as per Eq. (7), using OC solids samples collected before and after fueled operation on the last campaign day. This period captures the SPM fuel test and an unreported GWC fuel test (unreported due to operational upset during this test). The calculation is presented in Table 12.

The calculation in Table 12 accounts for the K introduced into the reactor system with the fuel feed (calculated from fuel feed rate and fuel K content) and the K captured by the ilmenite (calculated from the OC sample elemental analysis and an the average system inventory for the fueled period). The calculation confirms that>98% of the K introduced into the reactor system is absorbed by the Ilmenite oxygen carrier.

Comparison of the relative AR and FR alkali release rates shows that for BP and PFR fuel, roughly equivalent mass amounts of alkali are released both in the FR and AR flue gases. The measured concentration of alkali in the FR flue gas is much higher, but this is compensated by the fact that the AR gas flow rate is approximately 4 to 10 times higher than that of the FR. The results for BP fuel are roughly consistent with those reported for the 100 kW CLC unit fueled with BP fuel [24]. In both cases, the AR and FR release is below 2% of total incoming alkali, and the rough magnitude of the percent release in each reactor is roughly equivalent. The SPM fuel shows different behavior. On average, 0.98% of alkali are released to the FR, but only 0.14% of the incoming alkali are released in the AR. The seven-fold release of alkali in the FR is closer to the expected behavior, as the fuel is converted in the FR. For all cases, alkali release behavior is dominated by alkali absorption by ilmenite. It is possible that removing ilmenite's strong alkali absorption effect, by using an oxygen carrier with low affinity for alkalis, may reveal a completely different partitioning of alkalis between the AR and FR.

Beyond the alkali release partitioning findings discussed above, a significant data analysis effort was made in finding possible relationships between reactor operating parameters and the measured alkali concentration. The primary investigated parameters were the system OC inventory, system circulation, and the oxygen demand. However, no clear dependencies were observed, suggesting that Ilmenite's strong affinity for alkali and the fuel alkali content are the primary determinants of alkali emissions.

12.3. Conclusions:

In this study, a second generation 10 kW solid fuels CLC pilot system was commissioned with five different biomass fuels and ilmenite oxygen carrier. Commissioning tests showed that in order to achieve sufficient OC circulation, system inventory levels between 22 and 40 kg of ilmenite are required. Performance benchmarking tests were performed, leading to the following conclusions.

- The new system can achieve carbon capture efficiencies close to 100% for typical biomass fuels with Hight content of volatile matter, and higher than 94% for low-volatiles fuels.
- A carbon stripper, omitted in the new design, is not required for achieving high carbon capture efficiencies with biomass fuels.
- The new system exhibits improved gas conversion efficiency of black pellets fuel, when compared to performance of the previous generation system. The improvement is likely a result of implementing a volatiles distributor in the FR.
- Higher system circulation, controlled by the system OC inventory level and the AR air flow rate, improves gas conversion efficiency and solid fuels conversion efficiency of high-volatiles biomass fuels.

Measurement of AR and FR flue gas alkali emissions was conducted during the campaign, yielding the most complete characterization of gas-phase alkali release in CLC system presented to date. The following conclusions were made with respect to reactor alkali emissions measurements:

- The fate of alkali released during fuel conversion is dominated by absorption of approximately 96–99% of the fuel alkali by the ilmenite oxygen carrier.
- AR and FR flue gas emissions account for up to 3% of the alkali released from the fuel.
- Higher fuel alkali content results in higher alkali emissions in the FR flue gas. However, this effect is likely largely dampened by the strong absorption of alkali into the ilmenite bed material.
- AR alkali emissions are of the same magnitude as the FR alkali emissions for fuel with low alkali content. For the fuels with high alkali content, such as straw pellet mix (SPM), emissions from the FR are more than seven times greater than those from the AR. ilmenite's strong alkali absorption effect is thought to obfuscate the alkali release tendencies associated with other operational parameters.

CRediT authorship contribution statement

Ivan Gogolev: Conceptualization, Methodology, Validation, Fo, rmal analysis, Data curation, Writing - original draft, Visualization, Supervision. **Amir H. Soleimanisalim:** Investigation, Writing - review & editing. **Carl Linderholm:** Conceptualization, Investigation, Writing - review & editing, Supervision. **Anders Lyngfelt:** Conceptualization, Writing - review & editing, Supervision, Project administration, Funding acquisition.

Declaration of Competing Interest

The authors declare that they have no known competing financial interests or personal relationships that could have appeared to influence the work reported in this paper.

Acknowledgements

This work was carried out with funding from Swedish Research Council, project "Biomass combustion chemistry with oxygen carriers", contract 2016-06023, and by the Swedish Energy Agency, (grant number P43936-1) via the OxyCar-FBC project, which is a project performed within the framework of ERA-NET Bioenergy. Rebuild of 10 kW unit was supported by Carl Tryggers Stiftelse (Sweden), contract CTS 14:285.

References

[1] Lyngfelt A, Leckner B, Mattisson T. A fluidized-bed combustion process with inherent CO2 separation; Application of chemical-looping combustion. Chem Eng Sci 2001;56(10):3101–13.
[2] M. M. Hossain and H. I. de Lasa, "Chemical-looping combustion (CLC) for inherent CO2 separations-a review," Chemical Engineering Science, vol. 63, no. 18. Pergamon, pp. 4433–4451, 01-Sep-2008.
[3] A. Lyngfelt, M. Johansson, and T. Mattisson, "Chemical-looping combustion - Status of development," in CFB 2008 - Proceedings of the 9th Int. Conference on Circulating Fluidized Beds, in Conjunction with the 4th International VGB Workshop "Operating Experience with Fluidized Bed Firing Systems," 2008.
[4] Adanez J, Abad A, Garcia-Labiano F, Gayan P, de Diego LF. Progress in Chemical-Looping Combustion and Reforming technologies. Prog Energy Combust Sci 2012;38(2):215–82.
[5] Lyngfelt A. Oxygen Carriers for Chemical Looping Combustion - 4000 h of Operational Experience. Oil Gas Sci Technol 2011;66(2):161–72.
[6] A. Lyngfelt and C. Linderholm, "Chemical-Looping Combustion of Solid Fuels – status and recent progress," Energy Procedia, vol. 114, no. November 2016, pp. 371–386, 2017.
[7] A. Lyngfelt and H. Thunman, "Construction and 100 h of Operational Experience of A 10-kW Chemical-Looping Combustor," in Carbon Dioxide Capture for Storage in Deep Geologic Formations, Elsevier, 2005, pp. 625–645.
[8] Moghtaderi B. Review of the recent chemical looping process developments for novel energy and fuel applications. Energy Fuels 2012;26(1):15–40.
[9] M. Rydén, M. Hanning, A. Corcoran, and F. Lind, Oxygen Carrier Aided Combustion (OCAC) of Wood Chips in a Semi-Commercial Circulating Fluidized Bed Boiler Using Manganese Ore as Bed Material, vol. 6, no. 11. 2016.
[10] Abanades JC, et al. Emerging CO2 capture systems. Int J Greenh Gas Control 2015;40:126–66.
[11] Lyngfelt A, Brink A, Langørgen Ø, Mattisson T, Rydén M, Linderholm C. 11,000 h of chemical-looping combustion operation—Where are we and where do we want to go? Int J Greenh Gas Control 2019;88(June):38–56.
[12] Pachauri RK, et al. Climate change 2014: synthesis report. Contribution of working groups I, II and III to the fifth assessment report of the intergovernmental panel on climate change. Gian-Kasper Plattner 2014.
[13] Lyngfelt A. Chemical-looping combustion of solid fuels – Status of development. Appl Energy 2014;113:1869–73.
[14] T. Jenkins, B., Baxter, L., Miles, T. Jr., Miles, "Combustion properties of biomass, Fuel Processing Technology 54," pp. 17–46, 1998.
[15] Mims CA, Pabst JK. Alkali-catalyzed carbon gasification kinetics: Unification of H2O, D2O, and CO2 reactivities. J Catal 1987;107(1):209–20.
[16] Khan AA, de Jong W, Jansens PJ, Spliethoff H. Biomass combustion in fluidized bed boilers: potential problems and remedies. Fuel Process Technol 2009;90(1):21–50.
[17] Keller M, Leion H, Mattisson T. Mechanisms of solid fuel conversion by chemical-looping combustion (CLC) using manganese ore: catalytic gasification by potassium compounds. Energy Technol 2013;1(4):273–82.
[18] P. Basu, Biomass gasification, pyrolysis and torrefaction: Practical design and theory. 2018.
[19] Berguerand N, Lyngfelt A. Design and operation of a 10 kWth chemical-looping combustor for solid fuels – Testing with South African coal. Fuel 2008;87(12):2713–26.
[20] Davidsson KO, Elled A-L, Eskilsson D, Leckner B, Åmand L-E, Steenari B-M. Countermeasures against alkali-related problems during combustion of biomass in a circulating fluidized bed boiler. Chem Eng Sci 2008;63(21):5314–29.
[21] Gu H, Shen L, Xiao J, Zhang S, Song T. Chemical looping combustion of biomass/coal with natural iron ore as oxygen carrier in a continuous reactor. Energy Fuels 2011;25(1):446–55.
[22] Mendiara T, Abad A, de Diego LF, García-Labiano F, Gayán P, Adánez J. Biomass combustion in a CLC system using an iron ore as an oxygen carrier. Int J Greenh Gas Control 2013;19:322–30.
[23] Corcoran A, Marinkovic J, Lind F, Thunman H, Knutsson P, Seemann M. Ash properties of ilmenite used as bed material for combustion of biomass in a circulating fluidized bed boiler. Energy Fuels 2014;28(12):7672–9.
[24] Gogolev I, et al. Chemical-looping combustion in a 100 kW unit using a mixture of synthetic and natural oxygen carriers – Operational results and fate of biomass fuel alkali. Int J Greenh Gas Control 2019;88:371–82.
[25] Cuadrat A, Linderholm C, Abad A, Lyngfelt A, Adánez J. Influence of limestone addition in a 10 kWth chemical-looping combustion unit operated with petcoke. Energy Fuels 2011;25(10):4818–28.
[26] Linderholm C, Lyngfelt A, Cuadrat A, Jerndal E. Chemical-looping combustion of solid fuels – Operation in a 10 kW unit with two fuels, above-bed and in-bed fuel feed and two oxygen carriers, manganese ore and ilmenite. Fuel 2012;102:808–22.
[27] Schmitz M, Linderholm C, Lyngfelt A. Chemical looping combustion of sulphurous solid fuels using spray-dried calcium manganate particles as oxygen carrier. Energy Procedia 2014;63:140–52.
[28] Linderholm C, Lyngfelt A, Dueso C. Chemical-looping combustion of solid fuels in a 10 kW reactor system using natural minerals as oxygen carrier. Energy Procedia 2013;37:598–607.
[29] Schmitz M, Linderholm C, Hallberg P, Sundqvist S, Lyngfelt A. Chemical-looping combustion of solid fuels using manganese ores as oxygen carriers. Energy Fuels 2016;30(2):1204–16.
[30] Schmitz M, Linderholm CJ, Lyngfelt A. Chemical looping combustion of four different solid fuels using a manganese-silicon-titanium oxygen carrier. Int J Greenh Gas Control 2018;70:88–96.
[31] Schmitz M, Linderholm C. Chemical looping combustion of biomass in 10- and 100-kW pilots – Analysis of conversion and lifetime using a sintered manganese ore. Fuel 2018;231:73–84.
[32] P. Moldenhauer, C. Linderholm, M. Rydén, and A. Lyngfelt, "Experimental investigation of chemical-looping combustion and chemical-looping gasification of biomass-based fuels using steel converter slag as oxygen carrier," in Proceedings of the International Conference on Negative CO2 Emissions, 2018, no. C, pp. 1–17.
[33] Wellinger M, Biollaz S, Wochele J, Ludwig C. Sampling and online analysis of alkalis in thermal process gases with a novel surface ionization detector. Energy Fuels 2011;25(9):4163–71.
[34] Pushp M, Gall D, Davidsson K, Seemann M, Pettersson JBC. Influence of bed material, additives, and operational conditions on alkali metal and tar concentrations in fluidized bed gasification of biomass. Energy Fuels 2018;32(6):6797–806.
[35] Davidsson KO, Engvall K, Hagström M, Korsgren JG, Lönn B, Pettersson JBC. A surface ionization instrument for on-line measurements of alkali metal components in combustion: Instrument description and applications. Energy Fuels 2002;16(6):1369–77.
[36] Tran K-Q, Iisa K, Hagström M, Steenari B-M, Lindqvist O, Pettersson JBC. On the application of surface ionization detector for the study of alkali capture by kaolin in a fixed bed reactor. Fuel 2004;83(7–8):807–12.
[37] Berguerand N, Lyngfelt A. The use of petroleum coke as fuel in a 10 kWth chemical-looping combustor. Int J Greenh Gas Control 2008;2(2):169–79.
[38] Berguerand N, Lyngfelt A. Energy procedia operation in a 10 kW th chemical-looping combustor for solid fuel – Testing with a mexican petroleum coke. Energy Procedia 2009;1(1):407–14.
[39] Berguerand N, Lyngfelt A. Chemical-looping combustion of petroleum coke using ilmenite in a 10 kwth unit-high-temperature operation. Energy Fuels 2009;23(10):5257–68.
[40] Berguerand N. Design and operation of a 10 kW th chemical-looping combustor for solid. Fuels 2009.
[41] Markström P, Linderholm C, Lyngfelt A. Chemical-looping combustion of solid fuels – Design and operation of a 100 kW unit with bituminous coal. Int J Greenh Gas Control 2013;15:150–62.
[42] C. Linderholm and A. Lyngfelt, "Use of Manganese Ores as Oxygen Carriers in Chemical-Looping Combustors for Solid Fuels," in Proceedings of the 4th International Conference on Chemical Looping, 2016, pp. 1–14.
[43] Linderholm C, Schmitz M, Biermann M, Hanning M, Lyngfelt A. International journal of greenhouse gas control chemical-looping combustion of solid fuel in a 100 kW unit using sintered manganese ore as oxygen carrier. Int J Greenh Gas Control 2017;65:170–81.
[44] M. Schmitz, C. Linderholm, and A. Lyngfelt, "Operational Experience of CO 2 Capture Using Chemical-Looping Combustion of Biomass-based Fuels in a 100 kW Unit," in Proceedings of the 1st International Conference on Negative CO2 Emissions, 2018, pp. 1–13.
[45] Abad A, Adánez J, Cuadrat A, García-Labiano F, Gayán P, de Diego LF. Kinetics of redox reactions of ilmenite for chemical-looping combustion. Chem Eng Sci 2011;66(4):689–702.